Flame-Solid-Interaction: Thermo-mechanical analysis for a steady stagnation flow stoichiometric NH_3-H_2 flame at a plane wall

Chunkan Yu,[*,†] Thomas Böhlke,[‡] Agustin Valera-Medina,[¶] Bin Yang,[§] and Ulrich Maas[†]

†*Institute of Technical Thermodynamics, Karlsruhe Institute of Technology, Engelbert-Arnold-Str. 4, 76131, Karlsruhe, Germany*

‡*Institute of Engineering Mechanics, Karlsruhe Institute of Technology, Kaiserstrasse 10, 76131, Karlsruhe, Germany*

¶*College of Physical Sciences and Engineering, Cardiff University, Cardiff CF24 3AA, United Kingdom*

§*Center for Combustion Energy, Tsinghua University, Beijing 100084, China*

E-mail: chunkan.yu@kit.edu

Phone: +49 721 608 43996. Fax: +49 721 608 43931

Abstract

While thermo-mechanical analysis in solid and combustion processes in the gas phase are intensively studied separately, their interaction is less investigated. On one hand, the combustion system can be affected by the solid due to for example the heat conduction. On the other hand, the high temperature flame can induce the thermal load in the solid, which significantly affect the mechanical stress field in the material. This work focuses on the coupling between solid and flame, and the combustion-induced

mechanical stress in the material. The influence of the solid on the flame structures and properties and also the influence of the flame on the thermo-mechanical behavior in the solid are investigated. A stagnation flow NH_3-H_2-air flame to a plane wall is considered as representative model, which is simple but also realistic in many engineering condition. As a result, it is shown that the flame can affect the thermal stresses in the plane wall significantly, depending on the flow imposed strain rates, system pressure and hydrogen content in the mixture. Furthermore, it is also shown that the solid would also flow plastically under certain conditions such as high pressures.

Introduction

Combustion engineering applications such as gas turbines, combustion chambers and furnaces are widely used for power supply, where high temperatures experienced by combustion systems (in blades, vanes, diffusers, injectors, etc.) require the implementation of novel materials or thermal coating barriers. As pointed in Ref.,[1] there are several important requirements in the design of combustion devices:

- The fuel must be completed burnt to get a higher thermal efficiency. However, heat is released due to chemical reactions during the combustion process and the temperature can be far more than several thousands kelvin.

- The material must have sufficient high mechanical strength to achieve a desired lifetime. The flame temperatures inside the combustion chambers are usually high (typically higher than 1500 K), such that the consequent temperature difference in the structure may induce thermal stresses, leading to thermal damage and shorter material lifetimes.[2,3]

Therefore, the design engineer of combustion applications must consider the efficient consumption/combustion of fuel and meanwhile the resulting mechanical loads such as thermal stresses which may destroy the structure. Of course there are various other requirements

such as the H_2 embrittlement in the material (and nitration when using ammonia gas)[4] in the design, and one can refer to for example Refs.[1,5,6]

Studies on the mechanics and combustion processes are usually performed independently, and a coupling of both processes are less considered even for simple configuration.

In many combustion studies, the variation of solid properties such as surface temperature and heat conductivity is less considered in the numerical simulation of reacting systems. For example, in Ref.[7] Wu & Law studied the stagnation flows with combustion close to a plane wall. In order to minimize the influence of wall and its surface, they modify the system configuration by replacing the wall with cold nitrogen in order to suppress the effect of the solid. In Ref.,[8–10] the solid surface temperatures are set to be the boundary condition with fixed values in the numerical simulation of reacting system, and are taken from experimental measurements. However, the solid may have noticeable effect on the combustion properties. It is reported in Ref.[11] the importance of inclusion of the heat transfer for an impinging laminar flame jet to a flat wall, and in Refs.[12,13] that the variation of heat conductivity of the solid changes the flame structures and the combustion efficiency.

Although various studies have been made on the numerical investigation of thermal stresses in engineering applications, there is limited literature considering the detailed chemical reactions in the numerical simulation of the thermal analysis. In Ref.[2] the effect of thermal stress on creep lifetime for a gas turbine combustion is reported by using the ANSYS software and considering the chemical kinetics. However, in their simulation, an one-step reaction model[14] is applied, which significantly simplifies the combustion process.

Besides the limitation of the investigation on the flame-solid interaction, most high temperature resistant materials have been developed for natural gas based combustion fields, there is still a large knowledge gap to address the complex phenomena and practical impacts of using ammonia (NH_3) as fuel vector in these systems, since the ammonia is a potential zero carbon fuel providing the energy storage medium for renewable sources, and the low ignitability of ammonia can be improved by adding hydrogen as co-fuel.[15,16] Initial attempts

recorded by the US Army revealed that Inconels X, 600 and 713C suffered little deterioration when they ran an ammonia program for fuel substitution after second world war.[15] Similarly, recent developments conducted by Japanese groups at AIST, Fukushima, show how the use of zeolite/yttrium based coatings can also reduce degradation.[17] Other studies performed by Chaturvedi et al.[18] showed some of the complexities of employing a blend of ammonium nitrate/urea heated to high temperatures. Though this blend is more representative of fertiliser solution, these studies present ammonium nitrate/urea solution as a nitrogen-based low carbon fuel alternative. Furthermore, thermal decomposition of ammonium nitrate shares some NHx reaction chemistry routes and intermediate species with ammonia-based combustion.[18] Results show impacts on the material when expose to combustion of these blends. One study of stainless steels and nickel-base alloys, tested at 793 K and 10 MPa pressure for 100h, found that alloys containing >23% Cr were more resistant to corrosive attack of intermediate compounds.[19] Recent work[4] characterised various nickel-base alloys employed in the aerospace sector (eg. Inconel, Hastelloy and Nimonic) and the impacts they suffer during combustion of ammonia/hydrogen blends. The work was conducted using a swirling flame of low power (<10kW) over a 5 hrs duration period. Results denoted the appearance of a thick layer over most materials, with hydrogen permeating this layer and reaching the molecular structures of the base material. Further research is required, but the work denotes the potential of hydrogen embrittlement from these types of ammonia-based blends. Thus, it was evident through an extensive literature review that there are still many unknown parameters on the impacts of structural components (and material integrity) when ammonia combustion is employed.

This work focuses on the thermo-mechanical analysis for the solid coupled with the ammonia-hydrogen-air flame simulation, and the detailed chemical mechanism and detailed molecular transport model are used to model the real combustion process. The following questions will be addressed:

- How will the flame affect the thermo-mechanical stress field in the solid? To what

extent will they be affected with the variation of flame parameters such as strain rate and pressure?

- In the combustion design, the addition of reactive species such as hydrogen as co-fuel is an efficient approach to promote the ignitability of fuel and enhance the energy efficiency.[20–22] However, as shown in Ref.,[22] the increasing enrichment of hydrogen in gas mixture leads to higher temperatures. Hence, to what extent will the thermo-mechanical stress field be changed in the solid with higher content of hydrogen?

- Under which conditions would the solid more likely to begin with plastic deformation?

This work is structured as follows. The configuration of studied stagnation flow flame to a plane wall is firstly introduced, and the involved assumption and simplification in the model are outlined. Then the governing equations for both flame (gas phase) and plane wall (solid phase), and the coupling between both phases at the interface are presented. Afterwards, the numerical algorithm for the solution of governing equations is shortly discussed, and the system model including computational domain, gas mixture composition, applied chemical mechanism and the material selected for the plane wall are elaborated. Following all the theory parts, the numerical results on the stagnation flow flame to a plane wall are represented and discussed in details. Finally, the main conclusions will be summarized and an outlook for future work is suggested.

Modeling of stagnation flow flame coupled with plane wall and its governing equations

In the present work, we focus on stagnation flow flames to a plane wall, as shown in Fig.1. In this configuration, fuel and oxidizer are pre-mixed and flow out of the burner nozzle, and a flame impinging normal to a plane surface is observed.

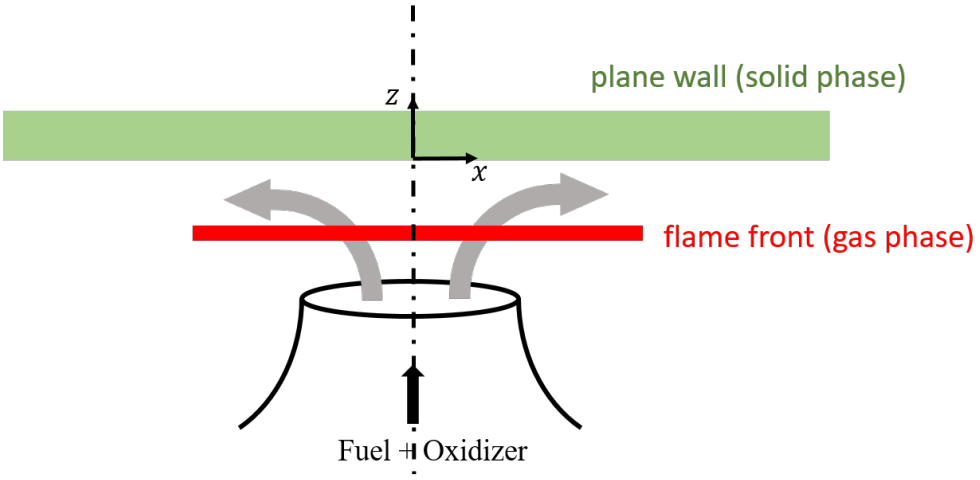

Figure 1: Schematical illustration of the studied stagnation flow flame to a plane wall

This configuration is frequently considered in the combustion community, because the corresponding experimental apparatus can be controlled easily and cost effectively.[8] Furthermore, it can be helpful to understand the flame-solid interaction in real engineering application such as the interaction between flame and blade in the gas turbine machinery.

In the following, several assumptions and simplification are made for the flame (gas phase) and the plane wall (solid phase):

- For flame in gas phase:
  - The flow in the burner can be assumed to be an axisymmetric stagnation flow, so that the flame can be approximated as one-dimensional with all thermo-kinetics quantities (e.g. temperature, species mass fractions) considered only in the symmetry line as functions of the z coordinate.
  - thermal radiation is neglected in the flame modeling. (Nevertheless, it could increase the thermal load of the solid, and modeling including thermal radiation is subject of future research.)
  - all thermo-physical properties are isotropic (uniformity in all orientations) but inhomogeneous (non-uniformity in spatial coordinate): they involve density ρ_g, isobaric specific heat capacity $c_{p,g}$, dynamic viscosity η_g, heat conductivity k_g and

molecular diffusion coefficients $D_{i,g}$ of species i. Here the subscript $_g$ represents the quantities for flame in gas phase.

- For plane wall in solid phase:
  - The strain is small such that the theory of linear thermoelasticity is valid.
  - The thermoelastic behavior is assumed to be isotropic.
  - The elastic parameters are temperature dependent. These properties involve mass density ρ_s, isochoric specific heat capacity $c_{v,s}$, heat conductivity k_s, coefficient of thermal expansion α_s , Young's modulus E_s, shearing modulus G_s.
  - The displacement and temperature fields in the plane wall are assumed to be only dependent on $z-$coordinate.
- At the interface of gas and solid phases:
  - surface reactions are not considered. In other words, the solid surface is considered as chemically inert. However, the effect of surface reactions on the flame structure and solid could be possible interesting issue which can be investigated in the future.[23]
  - there is no species diffusing into the solid. In other words, the molecular transport flux at the surface is zero.

Governing equations in the gas phase of a stagnation flow flame

The numerical computation of the stagnation flow flame follows the algorithm proposed in Ref.[24] Based on the boundary layer approximation (introduction of stream function), and introducing two parameters, the tangential velocity gradient G and the tangential pressure gradient J,[24] the governing equations can be reduced to a problem in one spatial coordinate, which is suitable for the description of stationary and unsteady flames. The corresponding mathematical equation system is expressed as

$$\frac{\partial \rho_g}{\partial t} = -2\rho_g G - \frac{\partial(\rho_g v_z)}{\partial z}, \tag{1}$$

$$\frac{\partial G}{\partial t} = -\frac{J}{\rho_g} - G^2 + \frac{1}{\rho_g}\frac{\partial}{\partial z}\left(\eta_g \frac{\partial G}{\partial z}\right) - v_z \frac{\partial G}{\partial z}, \tag{2}$$

$$\frac{\partial v_z}{\partial t} = -\frac{1}{\rho_g}\frac{\partial p_g}{\partial z} - \frac{4}{3\rho_g}\frac{\partial}{\partial z}(\eta_g G) + \frac{2\eta_g}{\rho_g}\frac{\partial G}{\partial z} + \frac{4}{3\rho_g}\frac{\partial}{\partial z}\left(\eta_g \frac{\partial v_z}{\partial z}\right) - v_z \frac{\partial v_z}{\partial z}, \tag{3}$$

$$\frac{\partial T_g}{\partial t} - \frac{1}{\rho_g}\frac{\partial p_g}{\partial t} = -\frac{1}{\rho_g c_{p,g}}\frac{\partial j_{q,g}}{\partial z} - \frac{1}{\rho_g c_{p,g}}\sum_{i=1}^{n_s} \dot{\omega}_i h_i M_i - v_z \frac{\partial T_g}{\partial z}, \tag{4}$$

$$\frac{\partial w_i}{\partial t} = -\frac{1}{\rho_g}\frac{\partial j_{i,g}}{\partial z} + \frac{\dot{\omega}_i M_i}{\rho_g} - v_z \frac{\partial w_i}{\partial z}, \tag{5}$$

$$0 = \rho_g - \frac{p_g \bar{M}}{R T_g}. \tag{6}$$

In these equations the gas mixture has the pressure p and temperature T_g. v_z is the flow velocity in axial direction. For $i-$th species, it has the mass fraction w_i, molar mass M_i, molar formation rate due to chemical reaction $\dot{\omega}_i$ (see Refs.[25,26] for details), energy transport flux $j_{q,g}$ and molecular transport fluxes $j_{i,g}$ in z direction, and the reacting system involves n_s number of reactive species. The tangential velocity gradient G is solely dependent on z-axis and formulated as

$$G(z,t) = \frac{v_x(z,t)}{x}, \tag{7}$$

where v_x is the flow velocity in radial direction (c.f. Fig.1). And the tangential pressure gradient J is written as

$$J = -\frac{1}{x}\frac{\partial p_g}{\partial x}. \tag{8}$$

As shown in Ref.,[24] the J is independent of z, and it is a constant quantity throughout the whole flow field.

For this two-parameter formulation, the strain rate imposed in the flow (which is related

to the outflow velocity) can be calculated as[24]

$$a = \sqrt{-\frac{J}{\rho_{\mathrm{g,ub}}}}, \tag{9}$$

where $\rho_{\mathrm{g,ub}}$ is the mixture density of unburnt gas.

The energy transport flux $j_{q,g}$ consists of two terms in the present work: one is attributed to the heat conduction $j^F_{q,g}$ which is described by Fourier's law; the other is attributed to the molecular transport of different species $j^D_{q,g}$. Thus the $j_{q,g}$ can be expressed as

$$j_{q,g} = j^F_{q,g} + j^D_{q,g} = -k_g \frac{\partial T_g}{\partial z} + T_g \sum_{i=1}^{n_s} c_{pi} j_{i,g}. \tag{10}$$

For the reacting system in gas phase, the molecular transport model plays a significant role.[27–30] Considering a detailed molecular transport model including the differential diffusion caused by different species, and the thermal diffusion (Soret effect: molecular diffusion due to temperature gradient), the mixture-average formulation for the diffusion fluxes $j_{i,g}$ is written as

$$j_{i,g} = j^D_{i,g} + j^T_{i,g} = -\rho_g D^D_{i,g} \frac{w_i}{x_i} \frac{\partial x_i}{\partial z} - \frac{D^T_{i,g}}{T_g} \frac{\partial T_g}{\partial z}, \tag{11}$$

where x_i is the mole fraction of $i-$th species. D^D_i represents the mixture-averaged diffusion coefficient, and D^T_i the thermal diffusion coefficient for the Soret effect. Both $D^D_{i,g}$ and $D^T_{i,g}$ are calculated according to Ref.[31] In this formulation, the diffusion coefficient for each species is not equal to each other: $D_{i,g} \neq D_{j,g}$ for $i \neq j$.

Note that other transport processes such as Dufour effect (heat transport due to concentration gradients) and pressure diffusion (molecular diffusion due to pressure gradient) are not included in the present work, because they are usually negligibly small in the combustion processes.[31]

Governing equations in the solid phase of a plane wall

For the numerical simulation in the solid phase of a plane wall, the the equation for heat conduction and equation of motion for solid are required. Before showing the general equations, it must be emphasized that all equations related to the solid mechanics here use index notation, and $i = 1$ means in $x-$direction, $i = 2$ in $y-$direction and $i = 3$ in $z-$direction, which is consistent with the equations used in the flame simulation.

In general, the equation for heat conduction and equation of motion for a isotropic thermo-elastic solid in spatial coordinate can be written in index notation as[32]

$$\rho_s c_{v,s} \frac{\partial T_s}{\partial t} = -\frac{\partial j_{q,i}}{\partial x_i} - T_s(3\lambda_s + 2\mu_s)\alpha_s \frac{\partial}{\partial x_i}\left(\frac{\partial u_i}{\partial t}\right) \tag{12}$$

$$\rho_s \frac{\partial^2 u_i}{\partial t^2} = \rho_s f_i + \frac{\partial \sigma_{ij}}{\partial x_j}, \tag{13}$$

where T_s is the solid temperature, u_i the displacement in $i-$th direction, f_i the body force, and λ_s and μ_s denote Lame's constants which are related to E_s and G_s by[32]

$$\lambda_s = \frac{\nu_s E_s}{(1+\nu_s)(1-2\nu_s)},$$
$$\mu_s = G_s = \frac{E_s}{2(1+\nu_s)},$$

where ν_s refers to the Poisson's ratio. The heat flux $j_{q,i}$ in Eq.12 is determined by the Fourier law as

$$j_{q,i} = -k_s \frac{\partial T_s}{\partial x_i}, \tag{14}$$

and the mechanical stress σ_{ij} in Eq.13 can be calculated through the constitutive equation for stress-strain relationships which reads[32]

$$\sigma_{ij} = 2\mu_s \epsilon_{ij} + \left[\lambda_s \epsilon_{kk} - (3\lambda_s + 2\mu_s)\int_{T_0}^{T} \alpha_s(T')\mathrm{d}T'\right]\delta_{ij}, \tag{15}$$

where δ_{ij} is the Kronecker-delta and ϵ_{ij} is the strain calculated through the symmetric part

of the displacement gradient as

$$\epsilon_{ij} = \frac{1}{2}\left(\frac{\partial u_i}{\partial x_j} + \frac{\partial u_j}{\partial x_i}\right). \tag{16}$$

Based on the assumption that the displacement field is only dependent on the $z-$coordinate and the displacement in $x-$ and $y-$directions disappear ($u_x = u_y = 0$), there exists no shear stresses in the plane wall ($\sigma_{ij} = 0$ for $i \neq j$). Thus the corresponding mechanical stress in the plane wall is reduced to

$$\underline{\underline{\sigma}} = \begin{pmatrix} \lambda_s \frac{\partial u_z}{\partial z} & 0 & 0 \\ 0 & \lambda_s \frac{\partial u_z}{\partial z} & 0 \\ 0 & 0 & (\lambda_s + 2\mu_s)\frac{\partial u_z}{\partial z} \end{pmatrix} - (3\lambda_s + 2\mu_s)\int_{T_0}^{T} \alpha_s(T')\mathrm{d}T' \begin{pmatrix} 1 & 0 & 0 \\ 0 & 1 & 0 \\ 0 & 0 & 1 \end{pmatrix}. \tag{17}$$

The displacement in $z-$direction (u_z) can be calculated through the equation of motion with the absence of body force as[32,33]

$$\rho_s \frac{\partial^2 u_z}{\partial t^2} = \frac{\partial}{\partial z}\left[(\lambda_s + 2\mu_s)\frac{\partial u_z}{\partial z}\right] - \frac{\partial}{\partial z}\left[(3\lambda_s + 2\mu_s)\int_{T_0}^{T} \alpha_s(T')\mathrm{d}T'\right], \tag{18}$$

and the temperature field in $z-$direction in the solid can be determined through[32,34]

$$\frac{\partial}{\partial t}\left(\rho_s c_{v,s} T_s\right) = \frac{\partial}{\partial z}\left(k_s \frac{\partial T_s}{\partial z}\right) - T_s(3\lambda_s + 2\mu_s)\alpha_s \frac{\partial}{\partial z}\left(\frac{\partial u_z}{\partial t}\right). \tag{19}$$

Note that the second term in the right hand side is the Gough–Joule effect which is usually negligible small[32].

After obtaining the mechanical stress $\underline{\underline{\sigma}}$ (see Eq.17), the von Mises equivalent stress σ_{vM} is determined by the Frobenius norm of the traceless part of the stress tensor as[35]

$$\sigma_{\mathrm{vM}}^2 = \frac{3}{2} s_{ij} s_{ij}, \tag{20}$$

where s_{ij} is the stress deviator determined by

$$s_{ij} = \sigma_{ij} - \frac{\sigma_{kk}}{3}\delta_{ij}. \tag{21}$$

For isotropic and incompressible plastic materials, the von Mises stress σ_{vM} represents an indicator for plastic yielding:[36–38] if it is less than the (tensile) yield stress, the loading is elastic; if the yield stress is reached then the material plastifies if the loading condition is satisfied.

Boundary Conditions

Figure 2 shows the whole computational domain, where $I_s = \{z| -H \leq z \leq 0^-\}$ is the domain for plane wall (solid phase) and $I_s = \{z|0^+ \leq z \leq \Omega\}$ for stagnation flow flame (gas phase).The interface of the solid and gas phases is at $z = 0$, corresponding to the stagnation plane for flow.

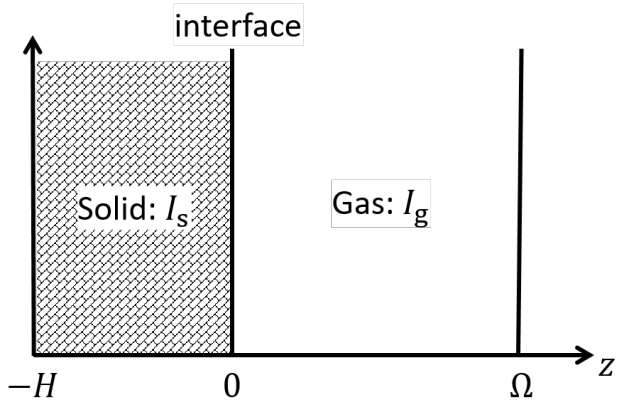

Figure 2: Schematic illustration of computational domain

In order to solve the governing equations introduced in the last section, boundary conditions are necessary at the left boundary ($z = -H$), at the right boundary ($z = \Omega$) and at the interface between flame and solid ($z = 0$).

At the left boundary ($z = -H$), the temperature of the solid is set to be a fixed value as $T_s(z = -H) = 300\mathrm{K}$, and the displacement here disappears $u_z(z = -H) = 0$.

At the right boundary ($z = \Omega$), the Dirichlet boundary condition is used for the flame simulation for species mass fractions $w_{i,\mathrm{ub}}$ ($i = 1, 2, \cdots, n_s$), temperature $T_{\mathrm{ub}} = 300\mathrm{K}$ and tangential pressure gradient J. The value of J is given via Eq.(9) for different strain rates.

At the interface between flame and solid ($z = 0$), it is the position of stagnation point (c.f. Fig.1), where $z = 0^-$ is from the solid side and $z = 0^+$ from the flame side. Because this position corresponds to a stagnation point, the flow velocity here is $v_z = 0$. Furthermore, since the plane wall is assumed to be impermeable, the species mass fractions must satisfy the condition that the molecular transport flux at this position must be zero

$$j_{i,g}(z = 0^+) = j^D_{i,g}(z = 0^+) + j^T_{i,g}(z = 0^+) = 0. \tag{22}$$

It should be especially emphasized here that, according to Eq.(11), the gradient of species mass fraction is not necessarily zero due to the differential diffusion of different species and additional term describing the thermal diffusion (Soret effect).

Furthermore, both sides share the same contact temperature T_c at the interface as

$$T_s(z = 0^-) = T_g(z = 0^+) = T_c, \tag{23}$$

and the energy transport flux at both sides of the interface must be the same

$$j_{q,s}(z = 0^-) = j_{q,g}(z = 0^+). \tag{24}$$

Recall that in the gas phase, the energy transport flux $j_{q,g}$ includes the energy transport caused by molecular diffusion $j^D_{q,g}$ (c.f. Eq.10). However, at the interface the molecular transport flux $j_{i,g}(z = 0^+) = 0$ (c.f. Eq.22) and thus $j^D_{q,g}(z = 0^+) = 0$, the condition for the heat flux Eq.24 can be reduced to

$$k_s \frac{\partial T_s}{\partial z}\bigg|_{z=0^-} = k_g \frac{\partial T_g}{\partial z}\bigg|_{z=0^+}. \tag{25}$$

Finally, the pressure of the flame flow at the stagnation point is balanced with the stress of the solid, which is expressed as

$$\sigma_{zz}(z = 0^-) = p_g(z = 0^+). \tag{26}$$

Numerical solution

Figure 3 summarizes the numerical coupling of both flame (gas phase) and plane wall (solid phase). The numerical simulation is performed using our in-house *INSFLA* code,[39] and has been validated for flame-wall interaction including complex surface reactions[23]. The *INSFLA* code has now been extended to solve the solid phase equations simultaneously. In the code, the *finite difference method* (FDM) is used for the spatial discretization, and the resulting *Differential-algebraic Equation* (DAE) system is solved using the extrapolation code LIMEX.[40] LIMEX can numerically compute DAEs with high stiffness. This is necessary because the chemical kinetics involve many elementary reactions with reaction rates of significantly different order of magnitude, leading to a high stiffness of the equation system.[41]

For the simulation of flame part, since the flame thickness is usually of order millimeter, much smaller than the computational domain ($0 \leq y \leq \Omega$), algorithm for an automatic adaptive mesh grid for the flame simulation is implemented. This meshing algorithm ensures sufficient grid points in regime where high scalar gradients occur. For the simulation in the plane wall, the mesh grid is uniform distributed.

In the *INSFLA* the unsteady governing equations for both gas and solid phases are solved simultaneously, coupled with the interface condition. They are the governing equations for the flame simulation Eq.(6), the equation of motion Eq.(18) and of temperature Eq.(19). Based on the information of the displacement u_z and temperature T_s of plane wall, the stresses $\underline{\underline{\sigma}}$ can be calculated via Eq.(17).

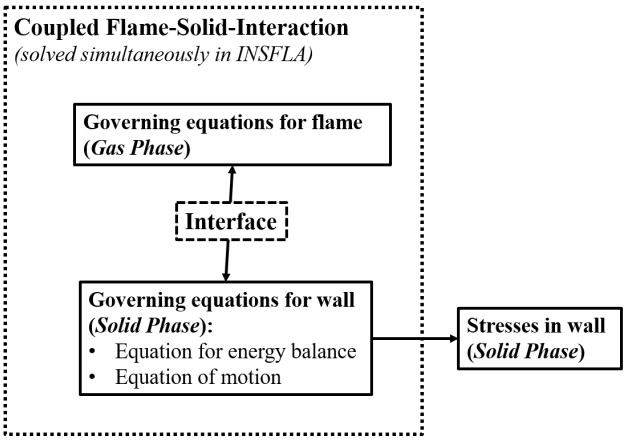

Figure 3: Schematic illustration of coupling of flame and wall simulation

Studied model system

Computational Domain

In the present work, the thickness of the plane wall is kept as 20 mm. The computational domain for the flame side is $\Omega = 0.15$m, which is sufficient large for all cases considered in the flame simulation.

Gas mixture and Chemical Mechanisms

The hydrogen-enriched ammonia combustion system is considered in the present work. In the recent combustion technique using ammonia, the addition of hydrogen can be up to 40% by volume, and a significant improvement of burning intensity can be observed.[16] In this work, we focus on the ammonia/hydrogen combustion system under stoichiometric mixture condition, and the level of H_2 addition in the ammonia is described by the mole fraction α_{H_2} of H_2 in the fuel as

$$\alpha_{H_2}H_2 + (1-\alpha_{H_2})NH_3 + \left(0.75 - \frac{\alpha_{H_2}}{4}\right)(O_2 + \frac{79}{21}N_2). \tag{27}$$

To perform the numerical simulation, the Li-2019 detailed chemical mechanism is used for the numerical simulation[42]. This mechanism has 34 species and 252 reactions for the

NH_3-H_2-air combustion system after removing all unnecessary species including hydrocarbon and inertgas such as AR and HE.

Material selected for the plane wall

In the present work, Ti-6Al-4V as titanium alloy is selected for the solid material, from which the plane wall is made. The Ti-6Al-4V titanium alloy is well-known for its high strength and good corrosion resistance, so that it is widely used in e.g. gas turbine and aerospace industry.[43,44]

In Fig.4 different thermo-physical properties of the material are outlined according to Tanigawa et.al.,[45] which are all functions of temperature as

- heat conductivity k_s in $\mathrm{W/(m \cdot K)}$:

$$k_s(T) = 1.1 + 0.017 \cdot \frac{T}{\mathrm{K}}. \tag{28}$$

- coefficient of thermal expansion α_s in $1/\mathrm{K}$:

$$\alpha_s(T) = \begin{cases} 7.43 \times 10^{-6} + 5.56 \times 10^{-9} \cdot \frac{T}{\mathrm{K}} - 2.9 \times 10^{-12} \cdot \left(\frac{T}{\mathrm{K}}\right)^2, & 300\mathrm{K} \leq T \leq 1100\mathrm{K} \\ 10.291 \times 10^{-6}, & 1100\mathrm{K} \leq T \leq 1300\mathrm{K} \end{cases}. \tag{29}$$

- Poisson's ratio ν_s:

$$\nu_s(T) = 0.2888 + 32.0 \times 10^{-6} \cdot \frac{T}{\mathrm{K}}. \tag{30}$$

- Young's modulus E_s in GPa:

$$E_s(T) = 122.7 - 0.0565 \cdot \frac{T}{\mathrm{K}}. \tag{31}$$

- Heat capacity $c_{v,s}$ in kJ/(kgK):

$$c_{v,s}(T) = 3.5 \times 10^2 + 8.78 \times 10^{-1} \frac{T}{\mathrm{K}} - 9.74 \times 10^{-4} \left(\frac{T}{\mathrm{K}}\right)^2 + 4.43 \times 10^{-7} \left(\frac{T}{\mathrm{K}}\right)^3. \tag{32}$$

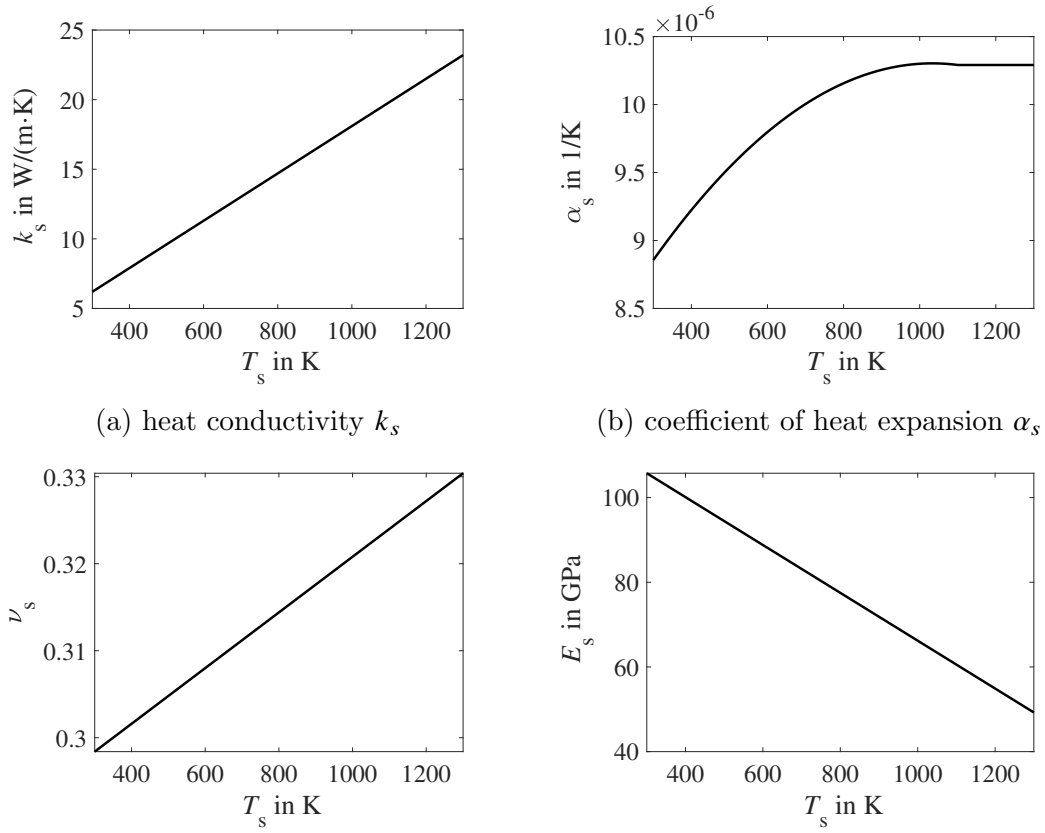

(a) heat conductivity k_s

(b) coefficient of heat expansion α_s

(c) poisson's ratio ν_s

(d) Young's modulus E_s

Figure 4: Properties of thermo-physical properties of Ti-6Al-4V

Although the temperature-dependent yield stress up to 1600K can not be found for Ti-6Al-4V to authors' knowledge, Li et.al.[46] provides an analytical solution to calculate the yield stress and is validated through different metallic materials. Therefore, the same analytical solution is also used to approximate the temperature-dependent yield stress for Ti-6Al-4V as

$$\sigma_Y(T) = \left[\frac{(1+\nu_s(T_0))E_s(T)}{(1+\nu_s(T))E_s(T_0)}\left(1 - \frac{\int_{T_0}^{T} c_{v,s}(T)\mathrm{d}T}{\int_{T_0}^{T_m} c_{v,s}(T)\mathrm{d}T}\right)\right]^{0.5} \sigma_Y(T_0), \tag{33}$$

where T_0 is any reference temperature and T_m the melting temperature. For Ti-6Al-4V,

according to the ASM Inc.,[47] the melting temperature is T_m = 1877 K, and the yield stress at reference temperature (T_0 = 298 K) is $\sigma_Y(T_0)$ = 880 MPa.

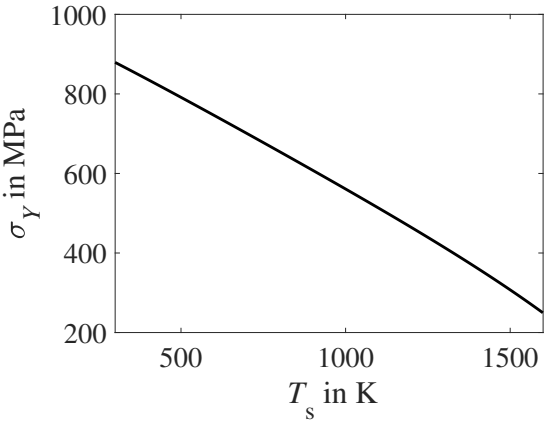

Figure 5: Temperature dependent compressive yield stress of Ti-6Al-4V according to Eq.33

Results and Discussion

In this section, diverse results concerning the flame-solid interaction will be discussed. Various model parameters will be varied. These are the strain rate imposed in the flame a, the system pressure p and the H_2 content in the gas mixture α_{H_2}. For all the following results discussion, the thickness of the wall is kept 20 mm, and we are only interested in the steady state, under which the maximum thermo-mechanical stresses are expected. Furthermore, we will focus on the von Mises stress σ_{vM}, which is an important indicator for the yield criterion.

Influence of flow strain rate a

Figure 6 represents first the influence of flow strain rate on the flame structure and on the von Mises stress in the solid σ_{vM}. Several observation can be made: First, consistent with the results already reported in combustion studies in e.g. Refs.,[48–50] the maximum of the flame temperature decreases monotonically with increasing strain rates. This is because

- with increasing strain rates the time-scales for the energy and molecular transport become shorter, so that the "degree of complete reaction" decreases;

- as strain rate increases, the flame is also imposed with a higher flow velocity, and the flame front (regime with maximum temperature) moves closer to the plane wall.[50,51] This leads to a larger heat flux $j_{q,\mathrm{s}}$ in the interface and also through the plane wall, which is shown in Fig.6(b). The increase of heat flux through the plane wall increases the heat loss of the flame system at the same time.

Second, as the flame front moves closer to the plane wall, one obtains a higher contact temperature T_c between solid and flame and consequently a higher σ_{vM} as shown in Fig.7(a). This means that for flame imposed with higher strain rate, although the maximum flame temperature decreases, the plane wall is subject to higher temperatures and higher stress.

As the strain rate is closely related to the turbulence intensity, namely flow with a higher turbulence is also imposed with a higher strain rate, the results shown here suggest that a strong turbulence could also aggravate the stresses loaded in the solid, since flames move more closer to the solid wall.

Influence of pressure p

In many engineering applications such as gas turbines or combustion engines, the whole combustion systems are operated under high pressures. Therefore, the combustion-induced mechanical stresses under high pressures are of great interest.

Figure 8 compares the maximum of the von Mises stress σ_{vM} in the plane wall against strain rates a under different pressures. The curves end up with extinction strain rate (ESR, a_E), above which no stable flames can be obtained. Regarding the pressure effect, we obtain two main issues.

First, if the flame flow is imposed under the same strain rate, the higher the pressure is, the greater $\sigma_{\mathrm{vM,max}}$ the wall is loaded. In order to explain this issue, Fig.9 shows the

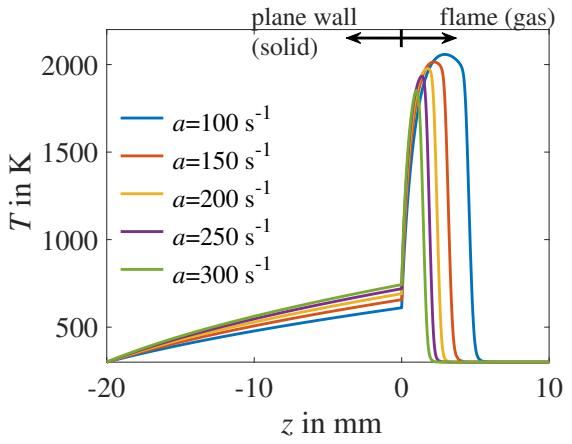

(a) temperature profile

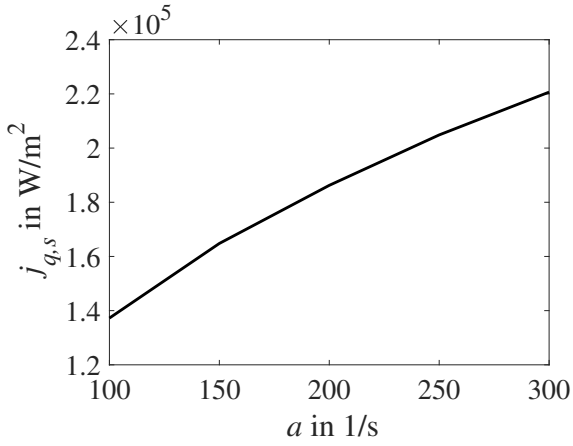

(b) heat loss $j_{q,s}$

Figure 6: Influence of strain rate on the flame temperature profile and heat loss in the plane wall. Gas mixture: stoichiometric condition with NH_3:H_2=0.6:0.4. p = 1 bar.

temperature profile (a) and max. von Mises stress $\sigma_{\mathrm{vM,max}}$ in the plane wall (b), if the flames are operated under different pressures but imposed with the same strain rates. From the temperature profiles of flames, it is observed that, as also reported from numerical simulation and experiment measurements in other literature,[52–54] the reaction zones of the flames (high temperature zones) become narrower with increasing pressures, which is attributed to decrease of mass diffusivities.[52,54] This leads to larger temperature gradients inside flames and, consequently, also larger heat flux flowing to the wall, if the pressures become higher. Therefore, the temperatures inside the wall become higher and the corresponding loaded max. von Mises stress $\sigma_{\mathrm{vM,max}}$ becomes larger. This phenomenon tells us that the mechanical stresses

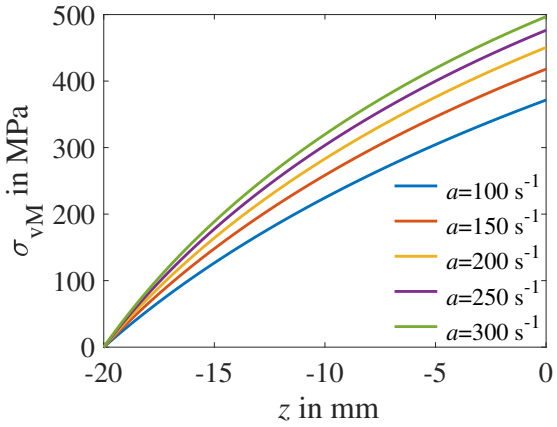

Figure 7: Influence of strain rate on the solid stresses from the flame. Gas mixture: stoichiometric condition with NH_3:H_2=0.6:0.4. p = 1 bar.

become more critical at high pressures.

Second, if one focuses on the extinction limit (the most right point of each curve), we observe that the increase of pressure would enhance the stoichiometric NH_3-H_2-air flame against extinction, which is also observed experimentally.[14,55] In order to examine the pressure effect on the flame and wall properties under the extinction limit condition, Fig.10 shows the counterplot of extinction strain rate a_E and the corresponding contact temperature between flame and wall T_c^E and the max. von Mises stress $\sigma_{\mathrm{vM,max}}^E$ over pressure and hydrogen content. It is clearly seen that under the extinction limit condition the T_c^E increases also with increasing pressure, leading to a monotonic increase of the mechanical stress loaded in the wall. For practice, the increase of pressure can extend the flame stability against extinction, but at the same time increase significantly the mechanical stress in the material.

Influence of H_2 content

It is already well-accepted that the addition of hydrogen in the ammonia mixture can overcome the shortcomings of the pure ammonia combustion system which has slow flame propagation, low flamability and long auto-ignition which inhibit large-scale usage. Therefore, the effect of addition of hydrogen on the induced mechanical stresses is investigated, and

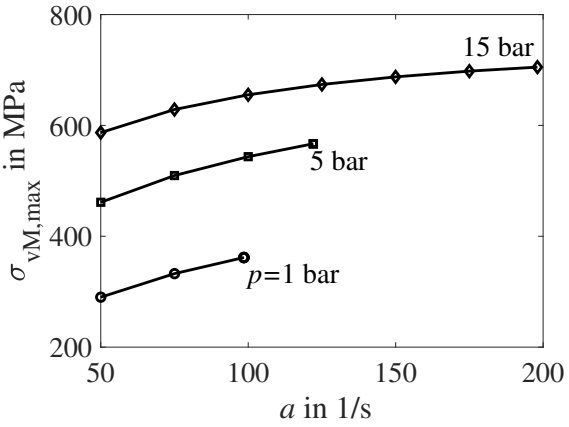

(a) NH_3:H_2=0.8:0.2

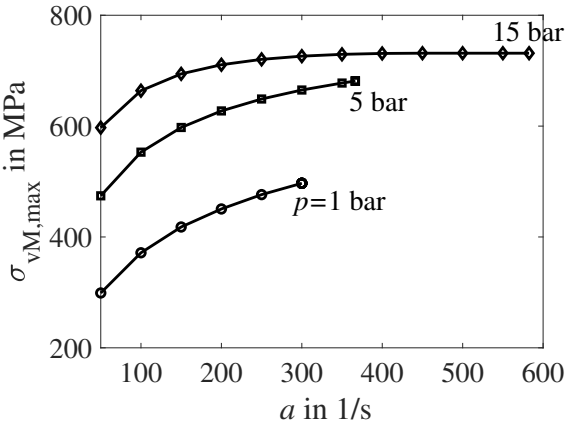

(b) NH_3:H_2=0.6:0.4

Figure 8: Dependence of maximum of the von Mises stress $\sigma_{\mathrm{vM,max}}$ against the strain rate for different pressures. Gas mixture: stoichiometric condition with two different hydrogen enrichment.

the maximum of the von Mises stress $\sigma_{\mathrm{vM,max}}$ against the strain rate for different hydrogen contents in the ammonia is shown in Fig.11.

It is clearly seen that for all considered pressures, the von Mises stress $\sigma_{\mathrm{vM,max}}$ varies only negligible small with hydrogen content. In order to understand this phenomenon, the temperature profiles in both wall and flame regimes are shown in Fig.12 where all four flames are imposed under the same strain rate and the pressure. The temperature distribution that is similar for all cases with different hydrogen content in the flame can be attributed to two different facts. From one side, the more hydrogen content is added into the ammonia gas, the

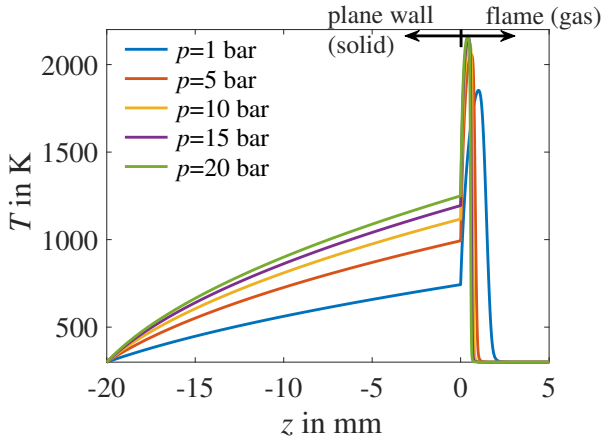

(a) temperature profile

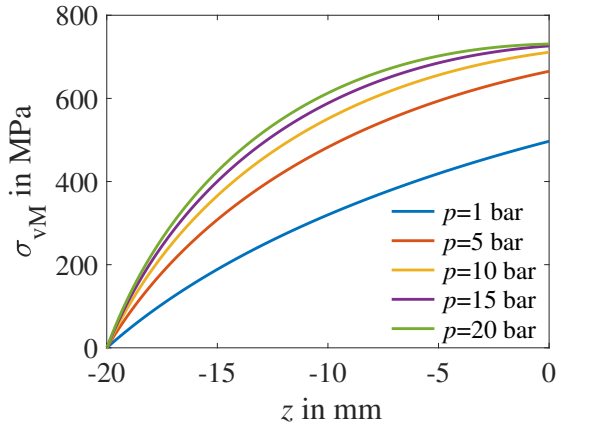

(b) von Mises stress σ_{vM} (solid phase)

Figure 9: Influence of pressure on the temperature profile (a) and von Mises stress σ_{vM} in the plane wall (b). Gas mixture: stoichiometric condition with NH_3:H_2=0.6:0.4. $a = 300\mathrm{s}^{-1}$.

higher the corresponding flame temperature is; From the other side, the chemical reaction rate becomes faster with increasing hydrogen content, leading to the flame front moving away from the plane wall. Both facts compensate with each other, and results in a similarity of the contact temperature between wall and gas and, consequently, the temperature distribution and the mechanical stress.

The investigation here shows a very important observation. The addition of hydrogen in the ammonia gas mixture can enhance the combustion efficiency (e.g. faster reaction rate, higher flame temperature) without causing larger mechanical stresses, if the flames are operated under the same flow conditions (e.g. the same strain rate). Moreover, the addition

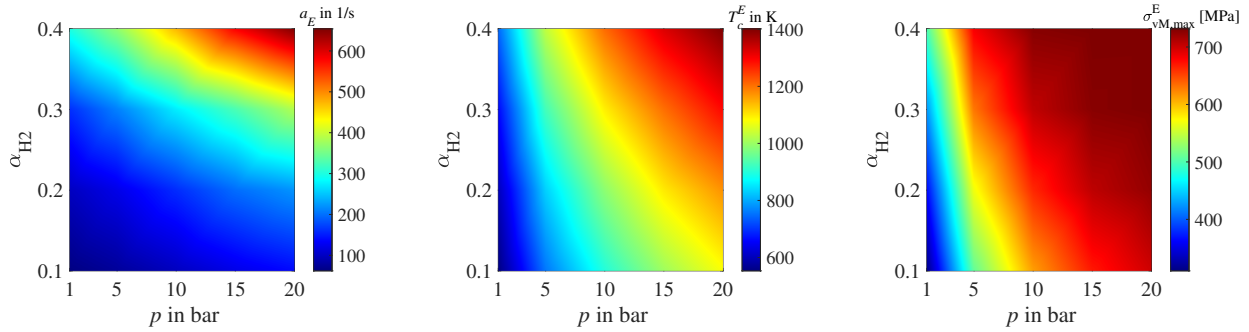

(a) ESR (b) contact temperature (c) max. von Mises stress

Figure 10: Counterplots of extinction strain rate a_E and the corresponding contact temperature between flame and wall T_c^E and the max. von Mises stress $\sigma^E_{\mathrm{vM,max}}$ over pressure and hydrogen content.

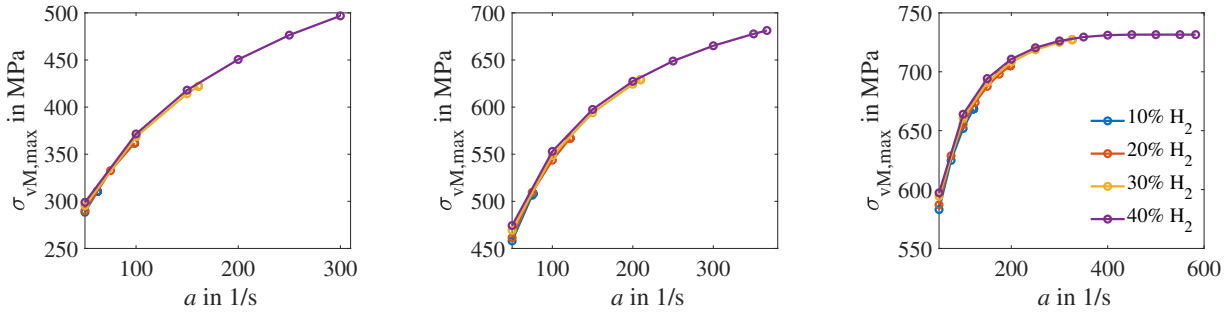

(a) p =1 bar (b) p =5 bar (c) p =15 bar

Figure 11: Dependence of maximum of the von Mises stress $\sigma_{\mathrm{vM,max}}$ against the strain rate for different hydrogen contents in the gas mixture under different pressures. Gas mixture: stoichiometric condition with two different hydrogen enrichment.

of hydrogen improves the flame stability against extinction from one hand, but increase the mechanical stresses under the extinction limit conditions from the other hand.

Comparison between the von Mises stress and yield stress

Till now, the influence of different combustion parameters on the mechanical stress field in the plane wall is investigated. As mentioned above, the von Mises stress is an indicator for plastic yielding for isotropic and incompressible plastic materials, therefore it is interesting to investigate whether the yield stress is reached under different conditions (in the thermolastic simulations here, plastic deformation is neglected). It should be emphasized here that the

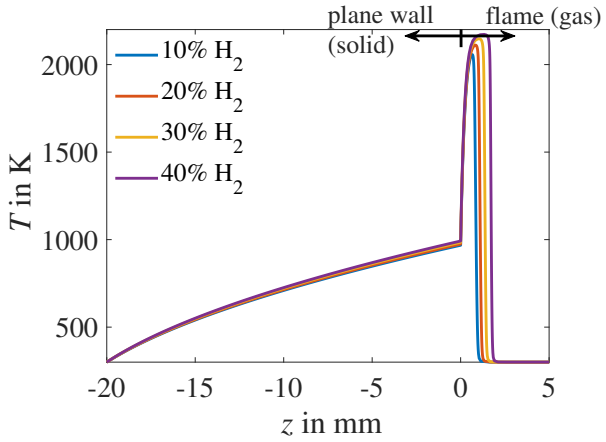

Figure 12: Influence of hydrogen content on the temperature profile. Gas mixture: stoichiometric condition. a=100s^{-1}. p = 15 bar.

yield stress determined according to the analytic solution (c.f. Eq.33 and Fig.5) is not validated for Ti-6Al-4V through experiments because of the measurement difficulty at high temperatures. Hence, the comparison between the von Mises stress σ_{vM} and yield stress σ_{Y} is rather qualitative.

Figure 13 shows the comparison between σ_{vM} and σ_{Y} for combustion system with stoichiometric mixtures of NH_3:H_2=0.6:0.4 at p = 1 bar. The flames are imposed with different strength of strain rates till their extinction limit a_E. It is observed that at this condition, the σ_{vM} at all locations in the plane wall is smaller than the yield stress, indicating that the loading is elastic and the deformed wall can return to its original shape when the combustion-induced thermal stress is removed.

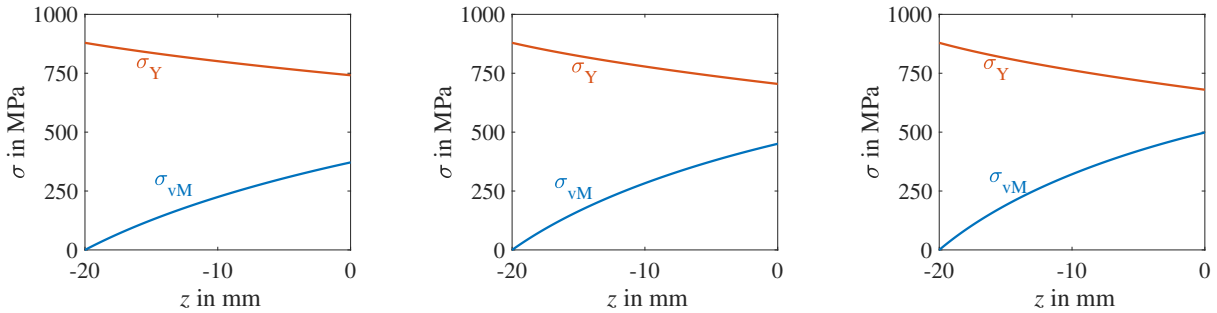

(a) a =100 s^{-1} (b) a =200 s^{-1} (c) $a = a_E$ =305 s^{-1}

Figure 13: Comparison between σ_{vM} and σ_{Y} for combustion system with stoichiometric mixtures of NH_3:H_2=0.6:0.4 at p = 1 bar.

The situation becomes more complicated, if one considers the comparison for the same combustion systems but at p = 15 bar, which is shown in Fig.14. Since the temperature inside the plane wall is much higher under high pressure combustion, the yield stress is reached in certain regime (e.g. for $-10\text{mm} \leq z \leq 0$ in Fig.14(b)). This gives us information that at this regime, walls can undergo a plastic deformation if the loading condition is satisfied and if the plastic flow would be modelled. Therefore the implemented equations (Eq.13 and Eq.15) in the present simulation, which are based on the assumption of linear thermoelasticity, are no longer valid. These results indicate that plastic or more accurate viscoplastic deformations should be included in the model approach in the future.

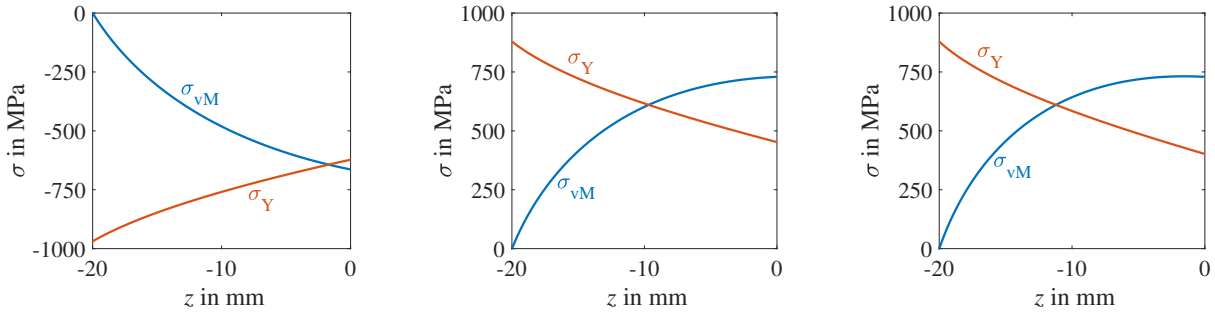

(a) a =100 s^{-1} (b) a =350 s^{-1} (c) $a = a_E$ =582 s^{-1}

Figure 14: Comparison between σ_{vM} and σ_{Y} for combustion system with stoichiometric mixtures of NH_3:H_2=0.6:0.4 at p = 15 bar.

Conclusions and Outlooks

In this work, the flame-solid-interaction is investigated, and the steady stagnation flow flame to a plane wall is selected as simple but representative configuration for the study. The NH_3-H_2-air combustion system is considered here and the wall made from the titanium alloy material (Ti-6Al-4V) are considered. It was mainly found that:

- An increase of flow strain rate leads to a decrease of flame peak temperature but, on the other hand, an increase of thermo-mechanical load in the wall since the flame moves closer to the wall, which is an opposite effect.

- The system pressure improves the flame stability against extinction, however the corresponding induced mechanical stresses increase also significantly.
- The addition of H_2 in the fuel improves the combustion efficiency (such as faster reaction rate, higher flame temperature), and keeps the thermo-mechanical stresses at the similar level.
- while at some conditions such as low pressures the von Mises stress is smaller than the yield stress, at other conditions such as higher pressures the yield stress can be reached and the material could undergo a possible plastic deformation if the corresponding loading condition is satisfied.

This work suggests that the consideration of the flame-solid interaction is an important topic for the thermo-mechanical analysis. In this work, only the steady state is considered. However, the transient processes would be also of interest since the variation of thermo-mechanical stresses would lead to additional mechanical issues such as fatigues. Furthermore, since the yield stress can be reached at some conditions, the plasticity should be modeled in the future, which renders the mechanical problem physically nonlinear.

Acknowledgement

This work was funded by the Deutsche Forschungsgemeinschaft (DFG, German Research Foundation) - Projektnummer 237267381 - TRR 150.

References

(1) Clarke, J. S.; Jackson, S. General considerations in the design of combustion chambers for aircraft and industrial gas turbines. *SAE Transactions* **1964**, 96–115.

(2) Moon, H.; Kim, K. M.; Jeon, Y. H.; Shin, S.; Park, J. S.; Cho, H. H. Effect of thermal

stress on creep lifetime for a gas turbine combustion liner. *Engineering Failure Analysis* **2015**, *47*, 34–40.

(3) Panakarajupally, R. P.; Presby, M. J.; Manigandan, K.; Zhou, J.; Chase, G. G.; Morscher, G. N. Thermomechanical characterization of SiC/SiC ceramic matrix composites in a combustion facility. *Ceramics* **2019**, *2*, 407–425.

(4) Kovaleva, M.; Dziedzic, D.; Mashruk, S.; Evans, S.; Valera Medina, A.; Galindo-Nava, E. The evaluation of ammonia/hydrogen combustion on the H permeation and embrittlement of nickel-base superalloys. 2022.

(5) Lefebvre, A. H. *Gas turbine combustion*; CRC press, 1998.

(6) Miles, P. C.; Andersson, Ö. A review of design considerations for light-duty diesel combustion systems. *International Journal of Engine Research* **2016**, *17*, 6–15.

(7) Wu, C. K.; Law, C. K. On the determination of laminar flame speeds from stretched flames. Symposium (International) on Combustion. 1985; pp 1941–1949.

(8) Bouvet, N.; Davidenko, D.; Chauveau, C.; Pillier, L.; Yoon, Y. On the simulation of laminar strained flames in stagnation flows: 1D and 2D approaches versus experiments. *Combustion and flame* **2014**, *161*, 438–452.

(9) Manuputty, M. Y.; Akroyd, J.; Mosbach, S.; Kraft, M. Modelling TiO2 formation in a stagnation flame using method of moments with interpolative closure. *Combustion and Flame* **2017**, *178*, 135–147.

(10) Hayakawa, A.; Hirano, Y.; Okafor, E. C.; Yamashita, H.; Kudo, T.; Kobayashi, H. Experimental and numerical study of product gas characteristics of ammonia/air premixed laminar flames stabilized in a stagnation flow. *Proceedings of the Combustion Institute* **2021**, *38*, 2409–2417.

(11) Remie, M.; Särner, G.; Cremers, M.; Omrane, A.; Schreel, K.; Aldén, L.; De Goey, L. Heat-transfer distribution for an impinging laminar flame jet to a flat plate. *International Journal of Heat and Mass Transfer* **2008**, *51*, 3144–3152.

(12) Wan, J.; Fan, A.; Yao, H.; Liu, W. Effect of thermal conductivity of solid wall on combustion efficiency of a micro-combustor with cavities. *Energy Conversion and Management* **2015**, *96*, 605–612.

(13) Zhang, H.; Chen, Z. Effects of heat conduction and radical quenching on premixed stagnation flame stabilised by a wall. *Combustion Theory and Modelling* **2013**, *17*, 682–706.

(14) Kim, K. M.; Yun, N.; Jeon, Y. H.; Lee, D. H.; Cho, H. H.; Kang, S.-H. Conjugated heat transfer and temperature distributions in a gas turbine combustion liner under base-load operation. *Journal of mechanical science and technology* **2010**, *24*, 1939–1946.

(15) Valera-Medina, A.; Xiao, H.; Owen-Jones, M.; David, W. I.; Bowen, P. Ammonia for power. *Progress in Energy and combustion science* **2018**, *69*, 63–102.

(16) Valera-Medina, A.; Amer-Hatem, F.; Azad, A.; Dedoussi, I.; De Joannon, M.; Fernandes, R.; Glarborg, P.; Hashemi, H.; He, X.; Mashruk, S., et al. Review on ammonia as a potential fuel: from synthesis to economics. *Energy & Fuels* **2021**, *35*, 6964–7029.

(17) Kurata, O.; Iki, N.; Inoue, T.; Fujitani, T.; Fan, Y.; Matsunuma, T.; Tsujimura, T.; Furutani, H.; Kawano, M.; Arai, K., et al. Pure Ammonia Combustion Micro Gas Turbine System. 2019 AIChE Annual Meeting. 2019.

(18) Chaturvedi, S.; Dave, P. N. Review on thermal decomposition of ammonium nitrate. *Journal of Energetic Materials* **2013**, *31*, 1–26.

(19) Starostin, M.; Grinberg Dana, A.; Dinner, O.; Shter, G.; Grader, G. High-Temperature

Corrosion of Stainless Steels and Ni Alloys During Combustion of Urea–Ammonium Nitrate (UAN) Fuel. *Oxidation of Metals* **2017**, *87*, 39–56.

(20) Sabia, P.; De Joannon, M.; Fierro, S.; Tregrossi, A.; Cavaliere, A. Hydrogen-enriched methane mild combustion in a well stirred reactor. *Experimental Thermal and Fluid Science* **2007**, *31*, 469–475.

(21) Fotache, C.; Kreutz, T.; Law, C. K. Ignition of hydrogen-enriched methane by heated air. *Combustion and Flame* **1997**, *110*, 429–440.

(22) Zhang, Y.; Fu, J.; Shu, J.; Xie, M.; Liu, J.; Jiang, T.; Peng, Z.; Deng, B. Numerical study on auto-ignition characteristics of hydrogen-enriched methane under engine-relevant conditions. *Energy Conversion and Management* **2019**, *200*, 112092.

(23) Strassacker, C.; Bykov, V.; Maas, U. REDIM reduced modeling of quenching at a cold wall including heterogeneous wall reactions. *International Journal of Heat and Fluid Flow* **2018**, *69*, 185–193.

(24) Stahl, G.; Warnatz, J. Numerical investigation of time-dependent properties and extinction of strained methane- and propane-air flamelets. *Combustion and flame* **1991**, *85*, 285–299.

(25) Warnatz, J.; Maas, U.; Dibble, R. W.; Warnatz, J. *Combustion*; Springer, 2006.

(26) Law, C. K. *Combustion physics*; Cambridge university press, 2010.

(27) Law, C. K. Heat and mass transfer in combustion: Fundamental concepts and analytical techniques. *Progress in energy and combustion science* **1984**, *10*, 295–318.

(28) Jayachandran, J.; Zhao, R.; Egolfopoulos, F. N. Determination of laminar flame speeds using stagnation and spherically expanding flames: Molecular transport and radiation effects. *Combustion and Flame* **2014**, *161*, 2305–2316.

(29) Ranganath, B.; Echekki, T. On the role of heat and mass transport during the mutual annihilation of two premixed propane–air flames. *International journal of heat and mass transfer* **2006**, *49*, 5075–5080.

(30) Jeon, J.; Shin, D.; Choi, W.; Kim, S. J. Identification of the extinction mechanism of lean limit hydrogen flames based on Lewis number effect. *International Journal of Heat and Mass Transfer* **2021**, *174*, 121288.

(31) Hirschfelder, J. O.; Curtiss, C. F.; Bird, R. B.; Mayer, M. G. *Molecular theory of gases and liquids*; Wiley New York, 1964; Vol. 165.

(32) Eslami, M. R.; Hetnarski, R. B.; Ignaczak, J.; Noda, N.; Sumi, N.; Tanigawa, Y. *Theory of elasticity and thermal stresses*; Springer, 2013; Vol. 197.

(33) Noda, N. Thermal Stresses in Materials with Temperature-Dependent Properties. *Applied Mechanics Reviews* **1991**, *44*, 383–397.

(34) Bird, R. B.; Stewart, W. E.; Lightfoot, E. N. *Transport phenomena*; Wiley, 2006.

(35) Mises, R. v. Mechanik der festen Körper im plastisch- deformablen Zustand. *Nachrichten von der Gesellschaft der Wissenschaften zu Göttingen, Mathematisch-Physikalische Klasse* **1913**, *1913*, 582–592.

(36) Boresi, A. P.; Schmidt, R. J.; Sidebottom, O. M., et al. *Advanced mechanics of materials*; Wiley New York, 1985; Vol. 6.

(37) Boothroyd, G.; Poli, C. *Applied Engineering Mechanics: Statics and Dynamics*; Routledge, 2018.

(38) Gross, D.; Ehlers, W.; Wriggers, P.; Schröder, J.; Müller, R. *Mechanics of Materials-Formulas and Problems*; Springer, 2016.

(39) Maas, U.; Warnatz, J. Ignition processes in hydrogen- oxygen mixtures. *Combustion and flame* **1988**, *74*, 53–69.

(40) Deuflhard, P.; Nowak, U. *Large Scale Scientific Computing*; Springer, 1987; pp 37–50.

(41) Goussis, D. A.; Maas, U. *Turbulent combustion modeling*; Springer, 2011; pp 193–220.

(42) Li, R.; Konnov, A. A.; He, G.; Qin, F.; Zhang, D. Chemical mechanism development and reduction for combustion of NH3/H2/CH4 mixtures. *Fuel* **2019**, *257*, 116059.

(43) Boivineau, M.; Cagran, C.; Doytier, D.; Eyraud, V.; Nadal, M.-H.; Wilthan, B.; Pottlacher, G. Thermophysical properties of solid and liquid Ti-6Al-4V (TA6V) alloy. *International journal of thermophysics* **2006**, *27*, 507–529.

(44) Niinomi, M. Mechanical properties of biomedical titanium alloys. *Materials Science and Engineering: A* **1998**, *243*, 231–236.

(45) Tanigawa, Y.; Akai, T.; Kawamura, R.; Oka, N. Transient heat conduction and thermal stress problems of a nonhomogeneous plate with temperature-dependent material properties. *Journal of Thermal Stresses* **1996**, *19*, 77–102.

(46) Li, W.; Zhang, X.; Kou, H.; Wang, R.; Fang, D. Theoretical prediction of temperature dependent yield strength for metallic materials. *International Journal of Mechanical Sciences* **2016**, *105*, 273–278.

(47) Ti, T. 6Al-4V (Grade 5). *STA, ASM, Aerospace Specification Metals, Inc. url: https://asm.matweb.com/search/SpecificMaterial.asp?bassnum=mtp641* **2022**,

(48) Sung, C.; Liu, J.; Law, C. K. Structural response of counterflow diffusion flames to strain rate variations. *Combustion and Flame* **1995**, *102*, 481–492.

(49) Law, C. K.; Sung, C.; Yu, G.; Axelbaum, R. On the structural sensitivity of purely strained planar premixed flames to strain rate variations. *Combustion and Flame* **1994**, *98*, 139–154.

(50) Egolfopoulos, F. N.; Zhang, H.; Zhang, Z. Wall effects on the propagation and extinction of steady, strained, laminar premixed flames. *Combustion and Flame* **1997**, *109*, 237–252.

(51) Bergthorson, J. M.; Salusbury, S. D.; Dimotakis, P. E. Experiments and modelling of premixed laminar stagnation flame hydrodynamics. *Journal of fluid mechanics* **2011**, *681*, 340–369.

(52) Som, S.; Ramirez, A.; Hagerdorn, J.; Saveliev, A.; Aggarwal, S. A numerical and experimental study of counterflow syngas flames at different pressures. *Fuel* **2008**, *87*, 319–334.

(53) Niemann, U.; Seshadri, K.; Williams, F. A. Methane, ethane, and ethylene laminar counterflow diffusion flames at elevated pressures: Experimental and computational investigations up to 2.0 MPa. *Combustion and Flame* **2014**, *161*, 138–146.

(54) Niemann, U.; Seshadri, K.; Williams, F. Effect of pressure on structure and extinction of near-limit hydrogen counterflow diffusion flames. *Proceedings of the Combustion Institute* **2013**, *34*, 881–886.

(55) Xiao, H.; Valera-Medina, A. Chemical kinetic mechanism study on premixed combustion of ammonia/hydrogen fuels for gas turbine use. *Journal of Engineering for Gas Turbines and Power* **2017**, *139*.